Available online at www.sciencedirect.com

SciVerse ScienceDirect

Polar Science 6 (2012) 23–37

NiPR National Institute of Polar Research

http://ees.elsevier.com/polar/

Analysis of satellite and model datasets for variability and trends in Arctic snow extent and depth, 1948–2006

Hotaek Park*, Hironori Yabuki, Tetsuo Ohata

Research Institute for Global Change, JAMSTEC, 2-15 Natushimacho, Yokosuka 237-0061, Japan

Received 17 June 2011; revised 3 October 2011; accepted 15 November 2011
Available online 22 November 2011

Abstract

This study aims to investigate the spatiotemporal trends in snow depth (SD) and snow cover extent (SCE) for Arctic lands, excluding Greenland, for the period 1948–2006. The investigation not only delineates how the Arctic regions are manifesting significant annual trends in both SD and SCE, but also provides a comprehensive understanding of their historical context. To achieve these objectives, the combined resources of the hydrological and biogeochemical model (CHANGE), National Oceanic and Atmospheric Administration (NOAA) weekly SCE data, and *in situ* observations of SD were used. Most regions in the Arctic exhibited a significant negative trend in SD over the 59 years of study. The magnitude of the negative trend was stronger in North America than in Eurasia, where the decrease became more significant, starting from the late 1980s, coinciding well with the temperature rise during that time. During the same period, the warming temperature caused a prominent decrease in deeper SDs (i.e., >35 cm), so that the corresponding SCEs exhibited negative anomalies, with the greatest declines being observed at SDs > 55 cm. In contrast, the SCEs for SD ≤ 35 cm showed increased anomalies during the most recent two decades. The increased anomalies signify a sequential result induced by the decrease in the SCEs with deeper SDs, rather than the expansion of snow to snow-free regions. These changes resulted in a northward shift of the shallow SD line, which took place to a highly significant degree in North America. These results suggest that the Arctic SCE and SD will undergo more intense changes in response to the future climate warming.

Keywords: Snow depth; Snow cover extent; Arctic lands; Spatiotemporal variability; Land surface model; Satellite data

1. Introduction

Snow is a vital component of the Arctic regions because its large seasonal variations and distinctive physical properties greatly affect climate, hydrology, and ecology at regional and global scales. The influence of snow on the Arctic system occurs through its interactions with other components within the system. Its influence produces manifestations that include positive albedo feedback (Groisman et al., 1994; Déry and Brown, 2007), along with other feedback related to moisture storage, latent heat, and soil insulation (Stieglitz et al., 2003). Snow-albedo feedback, which is linked to the radiative budget (Groisman et al., 1994), influences the temperature over a broad land surface, which in turn affects the atmospheric circulation and climate. This interaction has been cited as being a leading cause of increased warming in Arctic regions,

* Corresponding author. Tel.: +81 46 867 9292.
E-mail address: park@jamstec.go.jp (H. Park).

1873-9652/$ - see front matter © 2011 Elsevier B.V. and NIPR. All rights reserved.
doi:10.1016/j.polar.2011.11.002

especially in polar and mountainous regions (Serreze and Francis, 2006).

Snow depth (SD) is a key variable used to understand the evolution of the Arctic hydrological cycle. Arctic river discharge is mainly driven by the accumulated SD and depends on the timing of its melting, which may lead to extensive floods in spring (Yang et al., 2003). Climate change significantly influences the process of snow accumulation and ablation. Barnett et al. (2005) have projected that an acceleration of the hydrological cycle due to global warming in snow-dominated regions will expedite snowmelt and the occurrence of maximum SD, which could in turn lead to regional water shortages. The strong link between snow cover extent (SCE), SD, and river discharge has been investigated for Siberian watersheds (Yang et al., 2003) and northern Canada (Dery et al., 2005).

Recent research indicates a significant decrease in the snowfall over North America during winter, in response to rising air temperatures (Dyer and Mote, 2006). In contrast, long-term *in situ* measurements in Eurasia exhibit the trends of an increasing SD (Bulygina et al., 2009; Kitaev et al., 2005). These observations suggest that the Arctic regional snow depth response appears less consistent with the Arctic warming trend. However, very few *in situ* SD datasets for the Arctic regions are available and we have limited information with regard to spatiotemporal snow depth fields. Remote sensing techniques are used to complement the *in situ* data. For instance, satellite data have revealed that the Arctic spring SCE has experienced a rapid decrease since satellite observations were initiated, as has been well documented (Brown et al., 2010). The SCE derived from remote sensing images, however, provides information only about whether or not snow appears. Therefore, our knowledge of SCE only partially characterizes the actual snow variability. Unfortunately, very few studies have dealt with this variability with regard to the complete spatial coverage of the snow depth that has been evaluated over the Arctic region.

Although the Special Sensor Microwave/Imager (SSM/I) has provided radiometric measurements of snow depth changes over the Arctic land surfaces since 1989, the data record is perhaps remains too short to be useful for studies of interannual to multidecadal changes in SD. The weekly SCE charts from National Oceanic and Atmospheric Administration (NOAA) were derived from the manual interpretation of visible satellite imagery. The presence/absence of snow over the Northern Hemisphere was determined based on a 50% snow cover threshold for each grid cell. SSM/I-derived SCE includes large uncertainties/errors, especially in heavily vegetated areas (e.g., the boreal forest). Brasnett (1999) found that a lower threshold of 30% was required to emulate the snow covered area in the NOAA analysis, to ensure that the product has built-in conservatism, particularly in mountainous regions. Modeling presents a convenient and complementary approach to the assessment of spatiotemporal patterns of changes in the SD and SCE. Hirabayashi et al. (2005) reported, with the help of satellite-based observations, that the trends for snow covered areas over North America and Eurasia after the 1970s do not exceed the ranges of past variations that were produced by an off-line land surface model simulation for the years 1901–2000. Modeling results, however, also entail problems, as they are sensitive to forcing data and parameters. Therefore, the combined use of field observations, satellite data, and modeling results favorably expands the process of investigating SD and SCE trends in the Arctic on a continental scale. This combination of approaches also makes it possible to examine the degree of consistency between the satellite data and the modeling results in terms of the spatiotemporal variability of SD and SCE.

The main objective of this study is to investigate the spatiotemporal trends and variability in SD and SCE for the Arctic terrestrial regions, excluding Greenland, over a recent 59-year period (1948–2006), using a combination of land surface model simulation, satellite-based observations, and field observations. The investigation not only delineates how Arctic terrestrial regions are manifesting significant annual trends in both SD and SCE, but also provides a comprehensive understanding of their historical context. In addition, we see that variations in snowfall in response to climatic forcing can provide insight that might enable us to project the future variability of SD and SCE in response to climate change.

2. Model description

The combined hydrological and biogeochemical model (CHANGE) used in this study is a physically based land surface model designed to integrate the interactions and feedback effects in a soil-vegetation-atmosphere system in the Arctic terrestrial regions. CHANGE includes the following processes: spatiotemporal variations in the exchanges of energy, water, and CO_2 at the soil-vegetation-atmosphere interfaces; snow accumulation and melting; soil freezing and thawing; the effects of ice on soil water flux; the effects of soil organic matter on water and heat fluxes; and

vegetation dynamics, including the carbon and nitrogen budgets of the ecosystem. To integrate these interactions within a complex soil-vegetation-atmosphere system, CHANGE is designed to make use of a modular structure that consists of four modules, which cover land surface, vegetation phenology, carbon-nitrogen balance, and vegetation dynamics. Although a complete description of CHANGE is given by Park et al. (2011), the snow processes are briefly described here.

The land surface module essentially solves the energy and mass balances for the canopy, snow, and soil over a gridded domain. Therefore, snow processes are closely connected not only to radiation, energy, and the water budgets of the canopy layer and soil layers, but also to vegetation dynamics. The main snow processes represented in the model are shown schematically in Fig. 1. Because snowpacks are naturally layered media, CHANGE represents a snowpack as two layers: a thin surface layer and a thick deeper layer (Anderson, 1976; Wigmosta and Lettenmaier, 1994). The thin surface layer is used to solve the surface energy balance, while the thick, deeper layer is used to simulate deeper snowpacks. The surface energy balance components are used to simulate melting, refreezing, and changes in the snowpack heat content. The mass balance components represent snow accumulation or ablation, changes in the snow water equivalent, and the snowpack water yield. The snowpack energy balance is given by

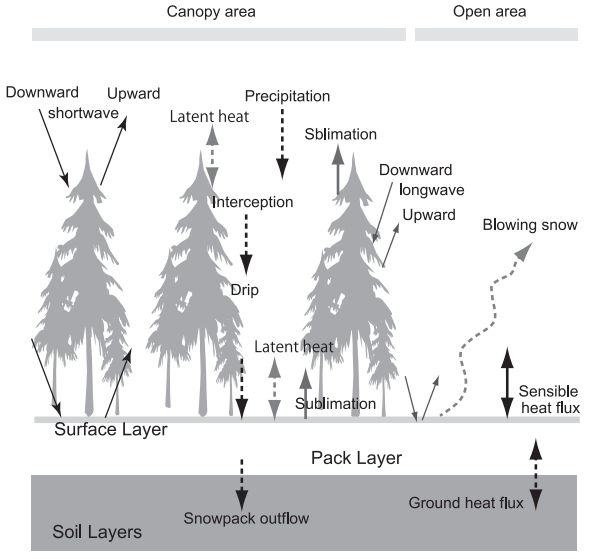

Fig. 1. Schematic of snow processes represented in CHANGE.

$$c_{ice}\rho_w \frac{\mathrm{d}w_{sp}T_{sp}}{\mathrm{d}t} = Q_n + Q_s + Q_l + Q_p + Q_m + Q_g, \qquad (1)$$

where c_{ice} is the specific heat of ice, ρ_w is the water density, w_{sp} is the snowpack water storage, Q_n is the net radiation, Q_s is the sensible heat transfer by turbulent convection, Q_p is the heat advected into the snowpack by rainfall, and Q_g is the heat transferred by conduction from the snow-ground interface. Further, Q_l is the energy lost to evaporation and sublimation or gained through latent heat release during condensation, while Q_m is the internal latent heat lost to melting or gained through liquid water refreezing. The left-hand term in Eq. (1) denotes the change in snowpack heat content. For the components on the right-hand side of Eq. (1) and the related equations, the reader can refer to Park et al. (2011). Eq. (1) is solved in time steps through a forward finite difference scheme in which the snow surface temperature (T_{sp}) is iteratively calculated.

The net radiation at the snow surface is calculated from the budget of the net shortwave and longwave radiations. Because the canopy and soil usually have different spectral properties for individual spectral bands, the shortwave radiation is decomposed into direct beam and diffuse radiation. The albedo is calculated for the canopy and the ground surface using a two-stream approximation method (Meador and Weaver, 1980), in which the overall direct beam and diffuse ground albedos are weighted, using combinations of the soil and snow albedos. The net radiation is divided into the right-hand terms of Eq. (1). The heat flux through the snowpack, Q_g, was added in order to combine the snow and frozen soil. Temperatures within a snowpack are assumed to follow a linear profile. However, taking into account the fact that the soil surface temperature is allowed to change, the balance of fluxes at the surface is given by

$$k_s \frac{\mathrm{d}T_{sp}}{\mathrm{d}SD} = G = -k \left.\frac{\mathrm{d}T}{\mathrm{d}z}\right|_{z=0}, \qquad (2)$$

where k_s is the thermal conductivity of snow (Jordan, 1991), $\mathrm{d}T_{sp}$ is the change in temperature from the snow surface to the ground surface, k is the thermal conductivity of the soil, and $\mathrm{d}SD$ is the change in the snowpack depth.

The total energy available from refreezing liquid water or for melting snowpack over a given time step depends on the net energy exchange at the snow surface, which is derived from Eq. (1) as:

$$Q_m = \left(Q_n + Q_s + Q_l + Q_p + Q_g\right)\Delta t \qquad (3)$$

If Q_m is negative, then energy is lost by the snowpack and liquid water (if present) is refrozen ($w_{sp,liq}$). If Q_m is sufficiently negative to refreeze all the liquid water, the snowpack may cool. If Q_m is positive, the excess energy produces snowmelt ($w_{sp,ice}$).

The mass balance of the snowpack takes into account two phases (liquid and ice) whose mass balances are given by

$$\Delta w_{sp,liq} = P_r + \frac{Q_l}{\rho_w \lambda_v} - \frac{Q_m}{\rho_w \lambda_f} \tag{4}$$

$$\Delta w_{sp,ice} = P_s + \frac{Q_l}{\rho_w \lambda_s} - \frac{Q_m}{\rho_w \lambda_f} \tag{5}$$

where λ_s and λ_v are the latent heats of sublimation and vaporization, respectively, P_r is the rainfall depth, and P_s is the water equivalent of the snowfall. Precipitation is partitioned into snowfall and rainfall based on the temperature threshold given by Wigmosta and Lettenmaier (1994). When $w_{sp,ice}$ exceeds the maximum thickness of the surface layer, the excess is distributed in the deeper pack layer. Similarly, the portion of $w_{sp,liq}$ that exceeds the liquid water holding capacity of the surface layer is drained to the pack layer. The liquid water remaining in the pack layer that exceeds the maximum holding capacity is immediately routed to the soil as snowpack outflow. However, since the temperature of the pack layer is below freezing, the liquid water in the pack is refrozen. During snowmelt, the atmosphere either exchanges water with the liquid phase, or it exchanges water vapor with the ice phase, in the absence of liquid water.

As snow accumulates on the ground, the snowpack compacts and its density increases over time. In addition to this increase in density, gravitational settling is caused by newly fallen snow, which further contributes to the densification of the snowpack over time. Following an approach similar to that of Anderson (1976), such compaction is calculated as the sum of the two fractional compaction rates that represent metamorphism and overburden. Metamorphism is an important factor for newer snow, but after the initial settling stage, the densification rate is controlled by the snow overburden through the load pressure. Within a layered snowpack, the load pressure differs for different pack layers, corresponding to their different compaction rates, which indicates that internal compaction is effective as load pressure.

Snow depth is not directly computed in CHANGE, but is needed for the calculation of the heat flux through the snowpack. Hence, the depth of the snowpack is simulated using a snow water equivalent (SWE), along with the density of the snowpack as influenced by compaction and metamorphism. That is,

$$\Delta SD = \frac{P_s \cdot SD}{SWE}\left[\frac{SD}{10}\right]^{0.35} \tag{6}$$

where ΔSD is the change in SD. The density of new snow is taken as 50 kg m^{-3} unless the air temperature is above 0 °C, in which case the snow density increases as a function of temperature (Anderson, 1976).

When snow falls, it is primarily intercepted by the canopy, where sublimation, mass release, and snowmelt occur. The processes of snow interception are included in CHANGE, based on the algorithm of Storck et al. (2002). The snowmelt from the canopy is calculated from the energy balance between the estimated surface temperature and the observed air temperature. The surface temperature of the canopy snowpack is solved iteratively with a modified energy balance, in a manner similar to that used for the ground snowpack (Eq. (1)). Snowmelt in excess of the liquid water holding capacity of the snow results in meltwater drip. Mass release from the canopy snowpack occurs if sufficient snow is available, and it is related linearly to the production of meltwater drip (Storck et al., 2002).

Separate aerodynamic resistances are calculated for the canopy, ground surface, and snow surface. When there is a canopy, the vertical wind velocity profile is modeled using three layers (Campbell, 1977). A logarithmic wind speed profile is used above the canopy. It is assumed that the wind speed decreases exponentially through the canopy, evolving into a new logarithmic profile near the ground or snow surface. When snowpack appears, the calculation of the turbulent energy exchange is complicated by the stability of the atmospheric boundary layer. If the snowpack is colder than the atmosphere (a stable condition), parcels of cooler air near the snow surface that are transported upward by turbulent eddies tend to sink back toward the surface, thus suppressing any turbulent exchange. In unstable (lapse) conditions, vertical motion is enhanced by buoyancy. Therefore, in the presence of a snowpack, the aerodynamic resistance is corrected for the atmospheric stability according to the bulk Richardson's number, which is a dimensionless ratio that relates the buoyant and mechanical forces (i.e., turbulent eddies) acting on a parcel of air (Anderson, 1976).

In wind-swept regions, snow transport by the blowing of wind causes snow cover redistribution and water loss as a result of sublimation fluxes. This transport and sublimation results in losses of from 30% to 75% of the annual snowfall in prairie, steppe, and

tundra regions (Pomeroy et al., 1997). Considering the importance of blowing snow, CHANGE is used jointly with an algorithm for blowing snow (Pomeroy and Li, 2000), which calculates the transport and sublimation fluxes using standard meteorological and land-cover data. Scaled-up blowing snow transport and sublimation fluxes are used to calculate open environment snow accumulation by accounting for the variability over open snowfields, increases in transport and sublimation with fetch, and the effect of exposed vegetation on partitioning the shear stress available to drive transport. The scaled blowing snow fluxes are used to calculate the snow mass balance and to simulate seasonal snow accumulation. Because the spatial resolution of the model is relatively coarse (0.5° × 0.5°), snow transport between grids is not considered in the simulation. Instead, all the snow transport caused by the blowing of wind is assumed to be the sublimation lost from the grid cell.

3. Model application and dataset

The CHANGE model was applied to the Arctic lands for the period 1948–2006 with a spatial resolution of 0.5° × 0.5°. The Arctic is defined as the land area north of 45°N and 0–360°E. Inputs to the model include information about vegetation type, soil texture, and atmospheric climate. The vegetation type in each grid cell was based on the vegetation map given by Ramankutty and Foley (1999), which recognizes 15 types of vegetation. Ice cover was not considered in the simulation, and thus Greenland was not included. CHANGE also requires soil texture information in terms of the fractions of sand, silt, and clay. We derived these data from the IGBP Soil Data System (Global Soil Data Task, 2000). The texture fractions were combined with soil organic matter data in order to estimate the thermal conductivity, heat capacity, and hydraulic conductivity of the soil. The gridded climate dataset used in this study had a global spatial resolution of 0.5° with a daily resolution from 1948 to 2006 (Hirabayashi et al., 2008; H08). This includes air temperature (mean, maximum, and minimum), precipitation, specific humidity, solar radiation, and wind speed. The gridded climate forcing was interpolated with station measurements of monthly temperature and precipitation (Hirabayashi et al., 2005). The monthly temperatures were obtained from Climatic Research Unit (CRU) Ts 2.1, and these were extended using the monthly gridded data from both the Global Historical Climatology Network (GHCN) and the NOAA CPC Climate Anomaly Monitoring System (CAMS). The monthly precipitation data included data from the NOAA CPC station and the Global Precipitation Climatology Centre (GPCC) ver. 5. The daily shortwave radiation product of the Surface Radiation Budget (SRB) was used to derive the data for the daily grid shortwave radiation forcing. Hirabayashi et al. (2005) well described the disaggregation of monthly climatic variables into a daily time series using a stochastic weather generator. The six-hourly surface-wind data for the period 1958–2001 from the European Centre for Medium-Range Weather Forecasts (ECMWF, ERA-40) were averaged in order to obtain daily values for each grid cell, and then the wind data of 2.5° × 2.5° were interpolated to 0.5° × 0.5°. The averaged daily grid wind was, in turn, averaged for the 365 (or 366) days of the year, based on the period 1958–2001. The averaged annual wind value was used for the remaining simulation years, except for the period 1958–2001. We downscaled this daily climate data to hourly data in order to accommodate the time step required by CHANGE. Park et al. (2011) have described well the hourly interpolation process for each variable. Park et al. (2011) also found that a constant diurnal relative humidity can cause a significant overestimation of the latent heat flux. Thus, an algorithm developed by Castellví et al. (1996) was used to interpolate the diurnal relative humidity.

The thermal and hydrological regimes of the ground and the vegetation components must be initialized for each grid cell. Since there are no detailed measurements for model initialization, the initial conditions were determined by spin-up runs. The initial assumptions included no snow, no soil carbon, and very little vegetation carbon. The initial soil moisture was set to 0.3 in all soil layers. The initial soil temperature profile was exponentially interpolated using the starting date air temperature at the surface and the mean annual air temperature at the bottom. The spin-up runs were repeated until the total ecosystem carbon flux reached a steady state after running for approximately 420 years, using the forcing data of the initial 20 years and a pre-industrial CO_2 concentration of 300 ppm.

We also used the NOAA weekly snow cover data to generate SCE time series over the Arctic regions for the period 1966–2006. The NOAA weekly product derived from manual interpretation of visible satellite imagery has been well described by Robinson et al. (1993). On the basis of these weekly records, we examined the monthly SCE variability within long-term time series. The long-term monthly SCE data were compared with the modeled SCE and were used to examine the relationship between SCE and SD.

The performance of SD as calculated by CHANGE was thoroughly investigated for a Siberian larch forest over a 9-year period (Park et al., 2011). However, the Arctic regions to which CHANGE was applied in this study have very different climates and land surface conditions. Before analyzing the trends of and the variability in SD and SCE, we first compared the simulated results with observations made under various conditions. The dataset of the Global Surface Summary of the Day (GSOD), which is archived at the National Climatic Data Center (NCDC, http://www.ncdc.noaa.gov/), includes SD data observed at meteorological stations worldwide. Thus, 518 stations that are located at >45°N and that recorded 10 or more years of SD data were selected for a comparison of the model results. The SD at each station was averaged over January to March (JFM) for each year of the period available.

4. Results and discussion

4.1. Climatic conditions

Winter (October to March) time series of air temperature and precipitation over the Arctic lands are shown in Fig. 2. The Arctic temperature exhibited an increasing trend, reaching 1.8 °C in 2002 and 1.62 °C in 2006, which are, historically, the warmest years on record. The years adjacent to these years were associated with the minimum Arctic sea ice cover. Over the last several decades, Arctic warming has become stronger, especially since the late 1970s (Fig. 2). Over the 59-year period, 1948–2006, the winter temperature increased 0.31 °C per decade, but the increase after 1979 was 0.42 °C per decade. Based on *in situ* observations over the Northern Polar Area (NPA), Bekryaev et al. (2010) found that the positive trends in NPA winter temperatures over longer time series were quite strong, with as much as 1.73 °C per century recorded for 1875–2008. The degree of warming since the late 1980s was stronger in the autumn and winter than in the summer (Fig. 3). During the same period, the temperature increase in the spring was also strong (Fig. 3).

Series of winter time precipitation exhibit a greater interannual variability than do winter time series for temperature. The strongest negative anomalies in precipitation were observed during the period 1948–1954, but after this, the anomalies became positive, reaching a maximum value in 1967. Beginning in 1970, the precipitation followed a cycle of increase and decrease that repeated on a timescale of 5–10 years. Among these precipitation cycles, those after 1995 displayed the greatest interannual variability. Precipitation showed a weak increasing trend during the period 1948–2006. However, this was not statistically significant. Precipitation during the 1948–1970 period showed a significant increasing trend at a ≥95% confidence level, while precipitation after 1990 tended to decrease.

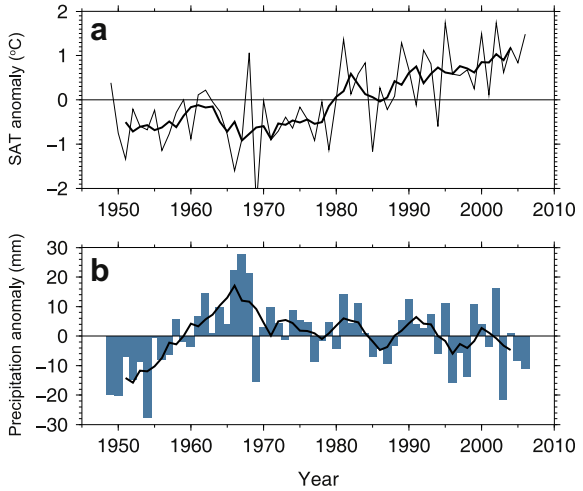

Fig. 2. Interannual variability of (a) winter time (October to March) surface air temperature (SAT) and (b) precipitation, during the period 1948–2006.

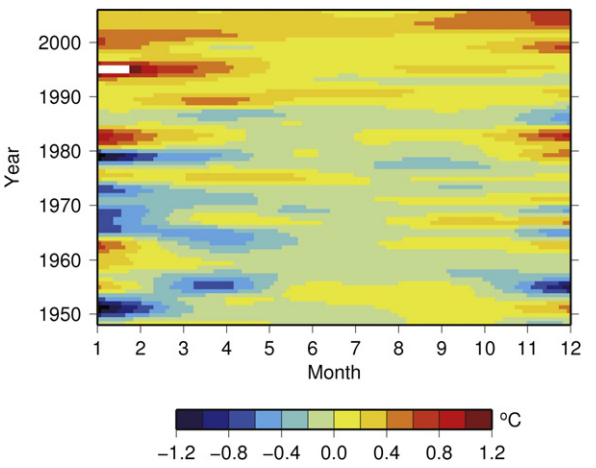

Fig. 3. Interannual variability of monthly surface air temperature anomalies over the Arctic lands during the period 1948–2006.

4.2. Comparison between simulations and observations of snow depth

The GSOD data included the daily SD at each site, which was averaged for JFM of individual years. The simulated SD was also averaged for the four grid pixels around the GSOD sites by weighting them for distance. The treated annual means of the observations and simulations were compared, and then, the correlation coefficients were derived from the comparisons at individual sites (Fig. 4). The correlation coefficients that were significant at a ≥95% confidence level are highlighted in color in Fig. 4a. Sites with significant correlation coefficients were mainly located inland, where the land cover was mainly classified as forest. At northern sites, where the density of SD observation stations was considerably lower, the correlations tended to be lower than at southern sites.

The annual JFM mean the SD at individual GSOD sites was in turn averaged over the period of availability. Correspondingly, the simulated values were averaged over the same period and found consistent with the observations. Fig. 4b compares the averaged SD results of the observations and simulations. Although the comparison reveals a large scatter, CHANGE estimates the SD moderately well. The deviation might be explained by the difference between the scale of the simulations and the observations. For complex terrains, point observations that are extrapolated to obtain large-area averages tend to be poorly representative of the true area means (Nelson et al., 1997). Scale issues are also encountered with differences in elevation, which fundamentally influence precipitation and temperature. Differences in land surface conditions are another reason for discrepancies between the simulations and the observations. Many GSOD sites measured SD in the open, while the grid pixels around the GSOD sites in the simulation were associated with forest. Therefore, the comparison should be viewed as a general assessment of model performance rather than a precise test.

4.3. Snow depth trends

The snow depth for JFM in the individual grid pixels was averaged over the period 1948–2006. Fig. 5a shows the spatial distribution of the averaged SD, which displays great regional heterogeneity. A linear regression analysis was performed on each grid for the annual SD averages during 1948–2006. The results of the trend analysis (Fig. 5b) show a great regional heterogeneity. During the study period, the snow depth generally exhibited a decreasing trend, except for local increases in regions of Western Siberia

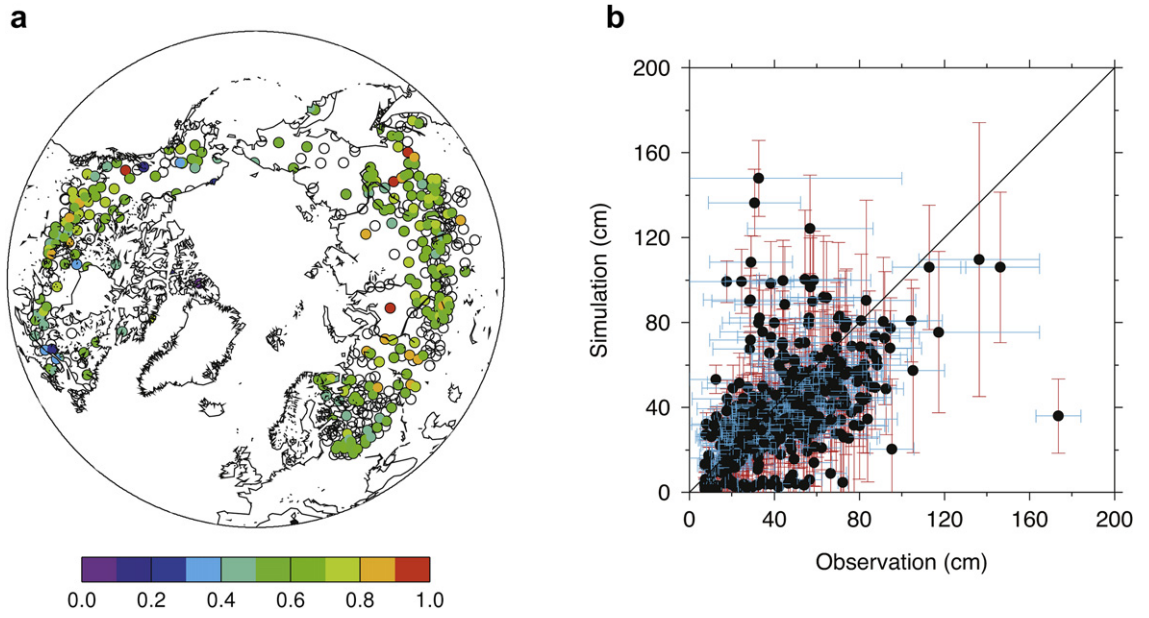

Fig. 4. (a) Location map of GSOD sites selected for validating the simulated snow depth. (b) Comparison between the observed and simulated snow depths averaged for JFM. In the map (a), the colors indicate the correlation coefficients of the observations and simulations at a ≥95% confidence level. In the plot (b), the horizontal and vertical bars represent the standard deviations of observations and simulations for snow depth, respectively.

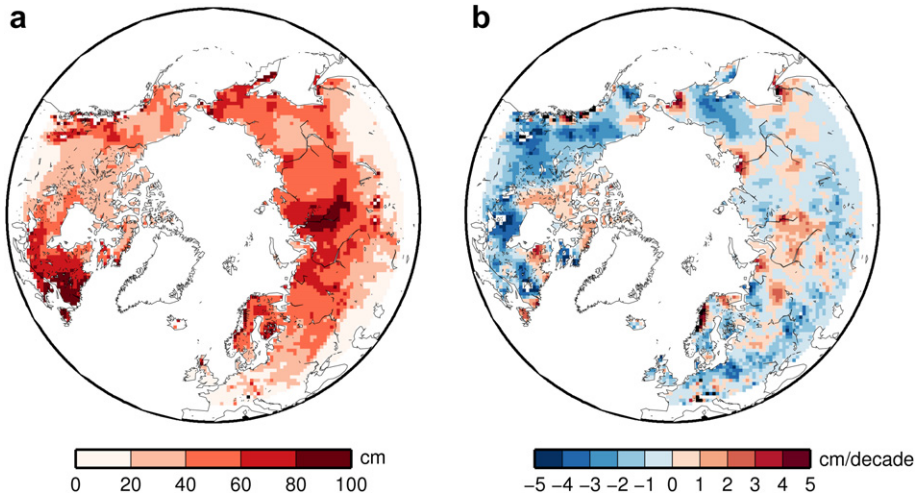

Fig. 5. (a) Distribution of average snow depth for JFM over the period 1948–2006. (b) The trend derived by a linear analysis.

(e.g., the Yenisey and Ob watersheds, in particular) and in the northwestern area of Hudson Bay (Fig. 5b). Bulygina et al. (2009) reported that the maximum SD at 820 *in situ* stations across Russia increased from 0.2 cm yr^{-1} to 0.6 or 0.8 cm yr^{-1} between 1966 and 2007 (with the maximum rates observed in Western Siberia). Based on *in situ* observations, Kitaev et al. (2005) found a positive SD trend (0.09 cm yr^{-1}) across Eurasia (for latitudes above 40°N) in February for the period 1936–2000. The increasing trend (<0.5 cm yr^{-1}) of the simulated SD in Siberian regions falls within the ranges derived from the observations. The decreasing trend of SD in the North American regions was stronger than for Eurasian regions. Dyer and Mote (2006) found locally significant decreases (>0.25 cm yr^{-1}) in the SD of northwestern Canada during 1960–2000. This decreasing SD over larger areas implies a response to rising air temperatures.

To integrally outline the spatiotemporal variability of SD during 1948–2006, we derived SD anomalies for 10-year intervals on a pixel-by-pixel basis (Fig. 6). Although some regions experienced below-average increases, the Arctic terrestrial regions generally had positive SD anomalies until 1980. In particular, both Western Siberia and the northwest regions of Hudson Bay exhibited an increasing trend during the 1948–2006 period (Fig. 5b). The Arctic coastal regions exhibited negative anomalies for 1951–1960, but these anomalies recovered to become positive for 1961–1970. Notably, the Arctic terrestrial regions were extensively covered by deeper snow in the period 1951–1980, during which the Arctic experienced negative temperature anomalies and much precipitation (Fig. 2).

There has been a distinct change in snow depth since 1980, when the SD predominantly shifted to negative anomalies, though some regions maintained weak positive anomalies until 1990. Thereafter, the negative SD anomalies in the Arctic regions became greater in both magnitude and extent. These negative anomalies were stronger in North America than in Eurasia. Satellite data reveal that since 1990, the SD has been decreasing over North America and has been increasing over Eurasia (Biancamaria et al., 2011). *In situ* observations have also addressed this decrease in SD over North America in recent years (Dyer and Mote, 2006), which may be the result of a combination of storm track and surface energy balance variability (Dyer and Mote, 2006). Isard et al. (2000) suggested that a positive phase of the Pacific North American (PNA) teleconnection during the winter (December–February) was correlated with the decrease in cyclone frequency in North America, and therefore with the decrease in SD. During the winter, a large area of central Canada is strongly influenced by an influx of Pacific moisture that is associated with a trough centered over the Gulf of Alaska, resulting in a strong southwesterly geostrophic flow into the southern Mackenzie River basin (Serreze et al., 2003). It has also been shown that the variability of SD is sensitive to the radiative balance (Groisman et al., 1994), surface energy fluxes (Dyer and Mote, 2002), and variations in air temperature (Brown and Goodison, 1996). The winter air temperature in North America exhibited an increasing trend over 15 recent years (Bekryaev et al., 2010), which led to a decrease in SD. Dyer and Mote (2007) found that the increase in

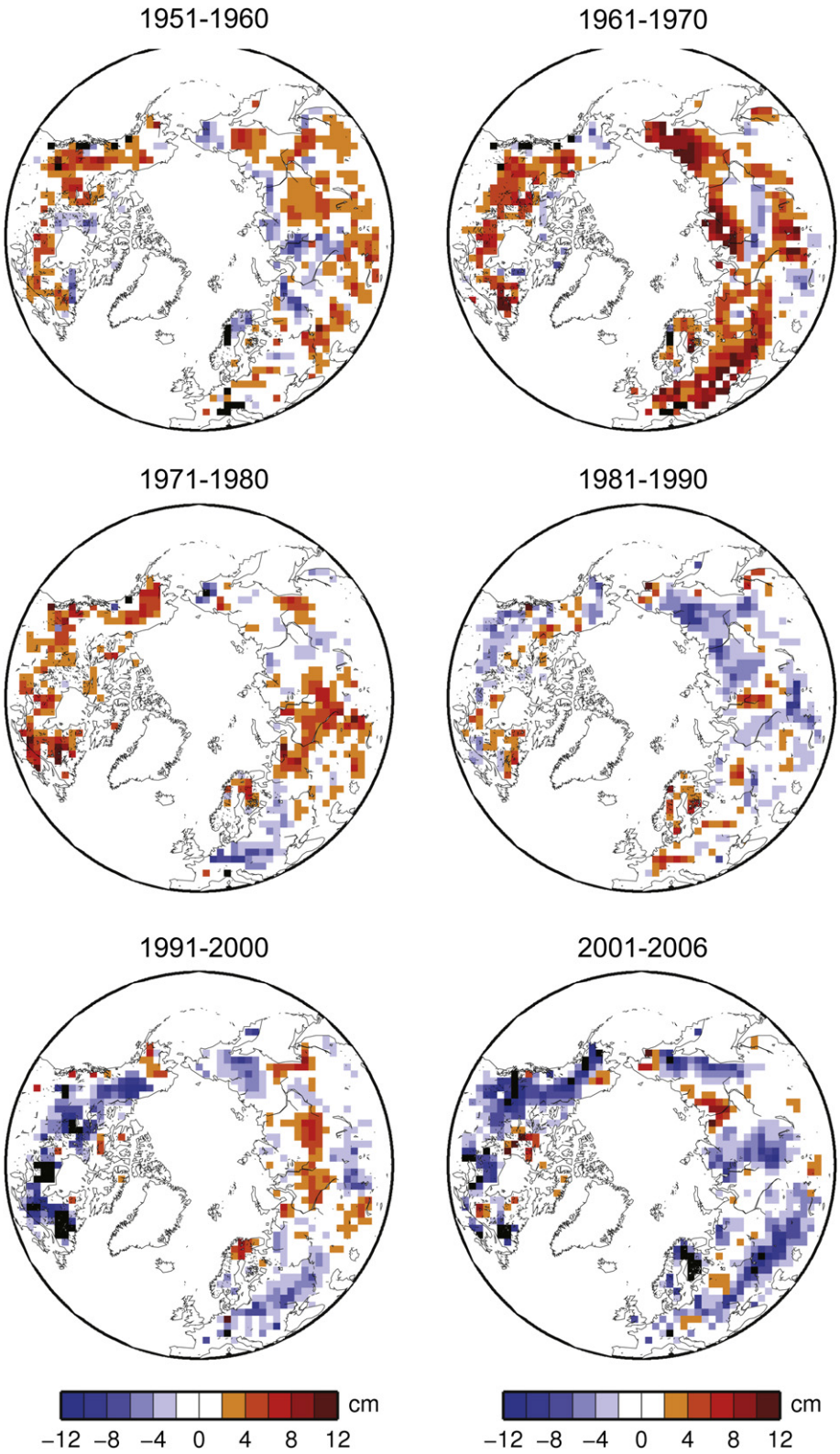

Fig. 6. Interdecadal variations in snow depth anomaly. Each anomaly is defined as the difference between the average during 1948–2006 and the average during the 10-year period.

the frequency of snow ablation events was a cause for the decrease in SD over North America.

Regions that exhibit anomalies contrasting with those of their neighbors can be found in the Ob, Yenisey, and Lena watersheds. Interestingly, these regions appear in most of the maps in Fig. 6, although the strength of their anomalies are different. This pattern of opposite anomalies in these regions has been significant since 1991. Serreze et al. (2003) outlined the characteristics of seasonal moisture circulations over these regions. According to their analysis, the variability in the winter effective moisture over the Ob is closely allied with the strength and location of the Urals trough, but variations in the winter precipitation in the Lena and Yenisey basins are more closely associated with the variability in the strength of the zonal flow. Moreover, the Eurasian watersheds (Ob, Yenisey, and Lena) have SD anomalies nearly opposite to those of the Mackenzie basin. Winter precipitation in the Mackenzie basin is lee-side cyclogenesis, associated with a stronger than average zonal flow and a persistent influx of Pacific moisture (Serreze et al., 2003). Therefore, SD over North America and Eurasia is significantly correlated to the PNA and the Arctic Oscillation (AO), respectively (Biancamaria et al., 2011).

Arctic warming resulted in later snow accumulation in the fall and earlier snowmelt in the spring (Fig. 7). A period of earlier snow accumulation lasted until the 1980s. After 1989, however, the cycle of the overall pattern of snow accumulation began later due to the warming (Fig. 3). This delay in snow accumulation became even more significant after 2000, with a maximum of 8 days over the Arctic terrestrial regions (53°–70°N). Arctic warming in autumn, as identified in Fig. 3, has been addressed by many studies (Bekryaev et al., 2010; Screen and Simmonds, 2010). Screen and Simmonds (2010) determined that the warming in autumn is closely related to the diminishing Arctic sea ice, whose influence extends to 45°N. Satellite-based analysis for 1972–2000 revealed no evidence of any systematic trend in the first snow date over the Arctic (Dye, 2002). However, *in situ* observations in Russia indicated a trend toward an earlier first snow in the period 1937–1994 (Ye, 2001). Ye (2001) explained that this earlier snowfall in autumn might be related to the decreasing trends of solar radiation and northern land surface air temperatures in autumn during the 1945–1986 period. These different trends in the autumn SD may be attributable to the difference in the study periods used in the said study and the present study.

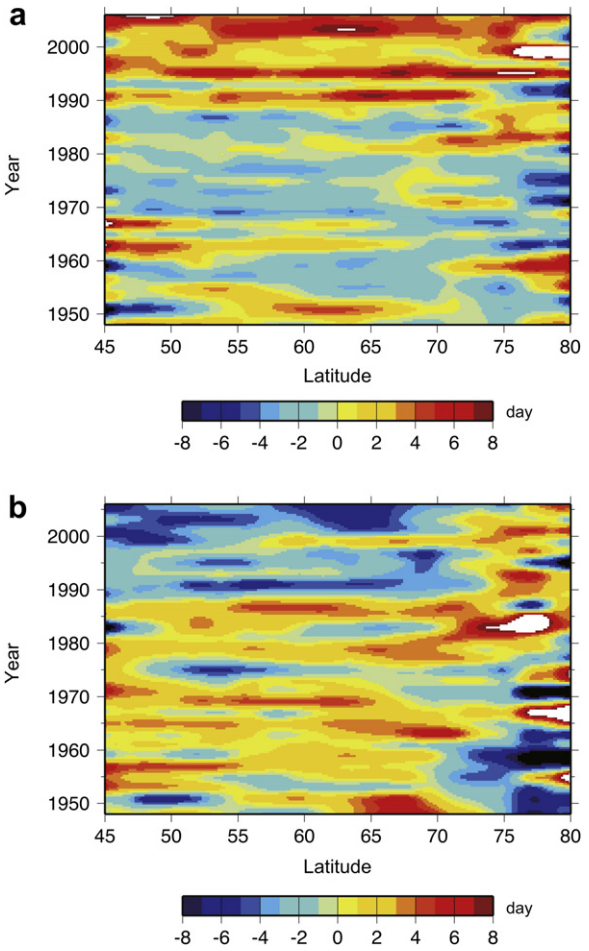

Fig. 7. Interannual variability of anomalies in (a) snow accumulation dates in the fall, and (b) snow disappearance dates in the spring. The white areas in high latitudes indicate the range-over of the maximum.

The earlier snowmelt in spring was mostly significant after 1990 (Fig. 7b), when the spring snow disappearance was earlier by a maximum of 8 days, which was indicative of the strong sensitivity to warming (Fig. 3). Evidently, both *in situ* observations (Dyer and Mote, 2006; Groisman et al., 2006) and satellite observations (Dye, 2002; Brown et al., 2010) captured the earlier snowmelt over the Arctic regions. Dye (2002) found that the spring snow disappearance over the Arctic was earlier by 3–5 days per decade for the period 1972–2000. Over central Canada, *in situ* observation-based gridded data have indicated that the regional decreases in spring snow depth are likely the result of a more rapid melting of shallower winter snowpacks (Dyer and Mote, 2006).

Effects related to the later first snowfall and earlier snowmelt have been found in various processes of the Arctic terrestrial ecosystems. The later snow

accumulation likely decreases the thermal insulation of the soil by snow (Iijima et al., 2010), while the earlier snowmelt can potentially cause earlier soil thawing (McDonald et al., 2004). In another finding, there was a negative correlation between the spring snowmelt dates and the normalized difference vegetation index (NDVI) of the growing season over central Siberia (Grippa et al., 2005), because the shorter growing season due to later snowmelt reduced the subsequent CO_2 capture in summer (Llody and Fastie, 2002). Both the later snowfall and the earlier snowmelt consequently lengthened the growing season, which may positively correlate to vegetation productivity. Changes in snowmelt patterns can also affect the associated peak floods and can thereby cause a shift in the hydrologic regime. In fact, a late snowmelt in Siberian watersheds has been associated with a high flood peak (Yang et al., 2003).

4.4. Snow cover extent trends

NOAA has provided weekly visible satellite observation data on Northern Hemisphere snow cover since 1966. Fig. 8a shows the monthly SCE time series over the Arctic during 1967–2006 for both the NOAA dataset and the model results. A comparison between the NOAA data and the simulated results shows good agreement for SCE (Fig. 8a). The monthly SD time series (Fig. 8b) were computed from the model results as the area-weighted average SD over the Arctic. Substantial differences can be observed in the seasonal and interannual variability of the two snow variables. The monthly mean SCE increases in the early snow season and reaches a maximum in January and February, but this increase exhibits almost no interannual variability, since the entire region is essentially covered in snow. The largest interannual variability of the monthly SCE occurs during the autumn snow accumulation and the spring snowmelt. Likewise, the SD over the Arctic is subject to interannual variability. However, the timing and magnitude of this variability does not necessarily correspond to the SCE, because SD shows a steadily increasing variation with accumulation, peaking in February and March. A relatively large interannual variability of SD can be observed during the peaks and the spring snowmelt season.

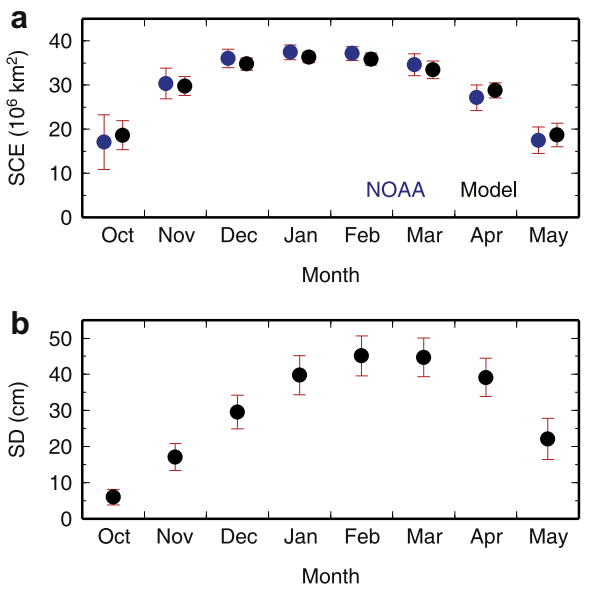

Fig. 8. Variations of (a) averaged monthly SCE derived from both NOAA weekly datasets and the model results, and (b) monthly snow depth based on the simulated results.

The different behaviors of these two snow parameters chiefly indicate that snow anomalies initially occur during the autumn accumulation and persist throughout the snow season. During the autumn or spring, the snow is of limited spatial extent and is generally shallow; thus, snowfall events and ablation processes affect both SCE and SD. During the midwinter season, the Arctic is covered by a relatively deep snowpack, and hence, abrupt changes in SCE are rare. SD, on the other hand, can be significantly altered by snowfall events and ablation processes in midwinter. These results suggest that SCE during autumn and spring is closely associated with SD (Ge and Gong, 2008). Satellite data have indicated that the mean SCE over the northern hemisphere was considerably less extensive after the mid-1980s than it was previously (Robinson et al., 1993; Groisman et al., 1994). The greatest negative anomalies of SCE occurred in the spring and early summer, due to the increased air temperature (Robinson et al., 1993; Brown et al., 2010). Analysis of the NOAA weekly dataset reveals clear evidence of stronger reductions in the spring snow cover in northern coastal regions (Brown et al., 2010), which likely coincide with enhanced local warming related to thinning sea ice (Lindsay et al., 2009) and earlier retreat of the sea ice (Howell et al., 2009). Similarly, the earlier snow disappearance over Arctic lands in spring has been identified for regions at 60°N and 70°N (Foster et al., 2008).

The variability of the monthly mean SD and SCE suggests that during the winter, SD does vary independently of the SCE, while the interannual variability of SD is likely associated with a variety of parameters. To ascertain the interannual patterns of SD over the

Arctic, a hybrid analysis of SD and SCE was performed with the simulated results (Fig. 9). Snow depth was classified into various levels, and SCE was defined as the areal extent of the snow cover at a given SD level. The SCE was averaged for individual SD levels during both the study period of 1948–2006 and the defined periods at 10-year intervals. The rate of SCE change indicates the ratio of the latter SCE average to the former. This analysis can provide information on the historical trend of SCE. Results of the SCE analysis, which show the interannual variability of SCE for individual SD levels, are presented in Fig. 9. The degree of variability was relatively high at lower ($\leq$5 cm) and higher ($\geq$66 cm) SD levels. At SD $\leq$ 5 cm, the SCE started increasing after 1971. For instance, the SCE during 2001–2006 increased by 62.2% as compared to the average. In contrast, the SCE at a level $\geq$66 cm changed from an increasing to a decreasing trend over the course of the time series, showing a maximum decrease during 2001–2006.

The SCE at most SD levels $\geq$36 cm exhibited negative anomalies after 1991, which is when the temperature entered a warming mode (Fig. 2a). Contrasting patterns are found at levels $\leq$35 cm (Fig. 9). Based on these findings, we defined an SD of 36–45 cm as the threshold level for SCE change that is related to climate change. Dyer and Mote (2006) found that in North America during 1960–2000, the most negative anomalies in SCE occurred at an SD level of 40–50 cm, with a second peak at 2–10 cm. These results are quite similar to ours. The increasing SCE of shallower snowpacks ($\leq$35 cm) over the most recent

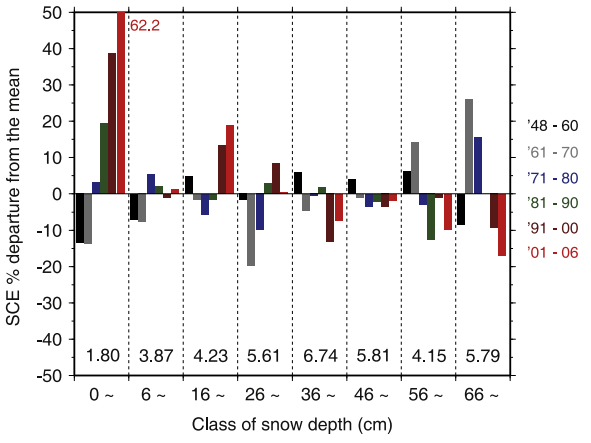

Fig. 9. Interannual variability of SCE over the Arctic lands at defined snow-depth levels. The numbers within the axes represent the average SCE (10^6 km^2) during 1948–2006, as calculated from the simulation results.

two decades is likely a result of the decrease in deeper snowpacks. To better illustrate these changes in SCE, the areal extent of snow cover for two SD levels ($\leq$5 cm and $\geq$36 cm) was compared for two periods: one with relatively deep snowpacks (1961–1970) and another with relatively shallow snowpacks (2001–2006). The comparison is presented in Fig. 10, in which the color brown represents instances when the SCE of each SD coexisted during the two periods. The color blue indicates the extended SCE during 1961–1970, relative to that during 2001–2006. Thus, blue and brown indicate the total SCE during 1961–1970, and green and brown collectively indicate the total SCE during 2001–2006. SCE at $\leq$ 5 cm (Fig. 10a) shifted considerably northward during the period 2001–2006, as opposed to 1961–1970, when an SD $\leq$ 5 cm hardly occurred. The northward movement of the snowline can explain the recent increase in SCE with a shallower SD. This implies the retreat of SCE at the thicker SD levels, rather than expansion of SCE into snow-free regions. In the case of SD $\geq$ 36 cm (Fig. 10b), the SCE during the period 2001–2006 declined considerably as compared to 1961–1970, most significantly in North America. These comparisons suggest that the increases in SCE with shallower snowpack during recent decades are the sequential result induced by declines in the occurrence of deeper snowpacks.

The significant negative anomalies in deeper snowpack have also been observed from *in situ* observations in North America (Brown, 2000; Dyer and Mote, 2006), and these have been correlated to both late snow occurrence and less precipitation. Moreover, the winter temperature increase may accelerate the advent of snowmelt. However, despite the negative SD anomalies identified for Eurasia during 2001–2006 (Fig. 6), no large decrease in SCE of $\geq$36 cm over Eurasia was discerned (Fig. 10b), even as it did decrease in some regions. The SD of the Eurasian regions highlighted in Fig. 10b was, on average, deeper than 35 cm (Fig. 5a). Therefore, the negative SD anomalies during the period (Fig. 6) are not as large an influence on SCE. However, the spring SCE is not necessarily consistent with the winter SD trend. During the snowmelt season, a deeper snowpack requires more energy in order for it to melt, and this might compensate for the greater availability of energy (sensible heat) that would otherwise act to melt the snow sooner (Foster et al., 2008). Satellite data indicate that the melting season over Eurasia has been beginning earlier, since the time observations were begun (Foster et al., 2008; Brown et al., 2010).

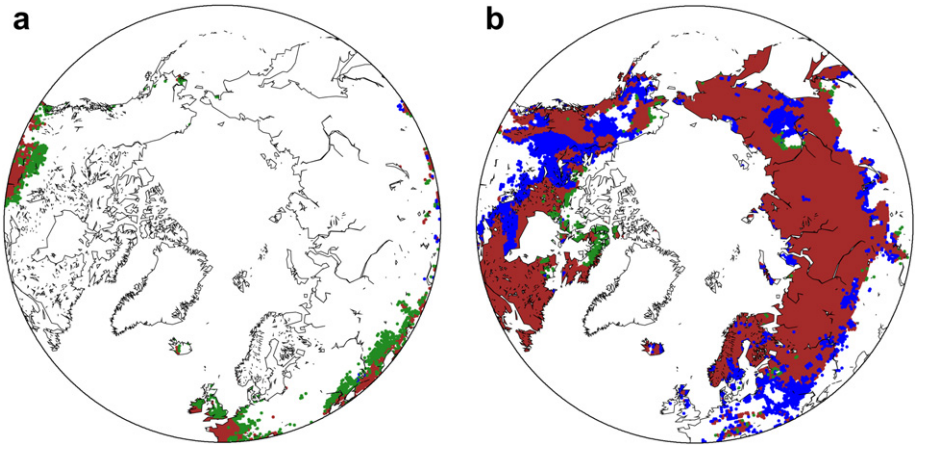

Fig. 10. Comparison between SCEs of 1961–1970 and 2001–2006 at snow depth levels of (a) <6 cm, and (b) ≥36 cm. The color brown indicates the area in which the SCE of each SD coexisted during the two periods. Blue and green indicate the extended area of SCE during 1961–1970 and 2001–2006, respectively.

4.5. Variability of SD and SCE in response to climate change

It is anticipated that snow cover will decrease in response to global warming, since snow accumulation and melting are highly sensitive to a temperature threshold of 0 °C. The rise in temperature has resulted in both later snow accumulation in fall and earlier melting in spring. Consequently, the duration of snow cover is shorter. These phenomena mostly become evident after the mid-1980s (Fig. 7), when the Arctic amplification became significant (Serreze and Francis, 2006). When Arctic warming is projected, increases in precipitation are predicted, especially at high latitudes and high elevations. An increase in precipitation is sufficient to offset reductions in the duration of the snow cover (Groisman et al., 1994). However, the resulting mild winters that accompany global warming might accelerate the onset of snowmelt, as has been identified in North America (Dyer and Mote, 2006). These changes would have regional sensitivities, since SCE and SD have presented a highly localized variability over the past 59 years. This suggests that a combination of the projected higher winter precipitation and earlier spring snowmelt might increase the frequency and severity of spring floods in the future environment of climate change.

Both the areal extent and the duration of snow cover are more closely linked to albedo feedbacks, which are stronger during the spring (Groisman et al., 1994; Déry and Brown, 2007). Earlier snowmelt in the spring enhances the available energy, increasing the surface temperature. This can affect the near-surface permafrost. Furthermore, a later snow accumulation combined with an earlier snowmelt allows for a longer active season of layer melting and thinner permafrost. In contrast, a shorter winter reduces the thermal insulation of soil by snow, the increasing the degree of soil freezing. However, the temperature increase during spring and summer might offset such freezing, since the higher soil moisture induced by the projected deeper snowpack could increase the soil's thermal conductivity.

The climatic impact of the Eurasian snow cover is not limited to a regional scale; interannual land surface snow anomalies in this region can influence the interannual variability of the winter mode of the AO (Saito and Cohen, 2003; Saito et al., 2004; Gong et al., 2004). However, the AO in JFM changed to a strongly positive mode in the late 1980s, which is consistent with the earlier spring snowmelt tendencies (Foster et al., 2008). This suggests that the resulting earlier snowmelt associated with global warming would have a compensatory positive impact on the AO.

5. Conclusion

This study examined the spatiotemporal trends in SD and SCE over the Arctic regions over a 59-year period and quantified the magnitude of their interannual variability using a combination of satellite observations and modeling results. Most regions in the Arctic exhibited a significant negative trend in SD over the 59 years, a trend that was significantly stronger in North America than in Eurasia. The patterns of the snow parameters in the snow season changed distinctly after the late 1980s

and are in good agreement with the warming patterns. During the same period, the SCEs of deeper snowpacks exhibited negative anomalies. The greatest decrease was identified at an SD $\geq$ 55 cm, while contrasting increases in SCE were observed at an SD $\leq$ 35 cm. The increase in the SCE of shallower SD in the two most recent decades is likely a dynamic that is induced by the decrease in the SCE of deeper SD. This reflects the northward shift of a shallower SD line, which was more significant in North America than in Eurasia.

The results of this study demonstrate that global warming has decreased both the SD and SCE in the winter. It is likely that these decreases contribute to the rapid snowmelt in spring. The decreases in SCE in the spring have consequences in the radiative balance. Due to variations in the net radiation induced by albedo feedback, the surface temperature increases, and therefore, soil thawing is enhanced. However, this study provides evidence that localized changes in SCE and SD occur, and that these changes affect regional hydrologic systems due to the change in the availability and release of snowmelt runoff. The localized variability of SD in the Arctic regions suggests uncertainty as to how future Arctic warming will affect snow processes. The dependence of precipitation, including snow, on atmospheric dynamics further increases the uncertainty of the magnitude or amplitude of future snow changes. However, it should be noted that earlier snowmelt of shortened duration, when combined with a thicker SD, could increase the frequency and severity of spring floods in the future.

Acknowledgements

We would like to thank two anonymous reviewers for their constructive comments on this paper. Forcing dataset for the model was provided by Dr. Y. Hirabayashi (Univ. of Tokyo).

References

Anderson, E., 1976. A Point Energy and Mass Balance Model of a Snow Cover. Tech. Rep. 19. National Oceanic and Atmospheric Administration, Washington, D.C.

Barnett, T., Adam, J., Lettenmaier, D., 2005. Potential impacts of a warming climate on water availability in snow-dominated regions. Nature 438, 303–309.

Bekryaev, R., Polyakov, I., Alexeev, V., 2010. Role of polar amplification in long-term surface air temperature variations and modern Arctic warming. J. Clim. 23, 3888–3906. doi:10.1175/2010JCLI3297.1.

Biancamaria, S., Cazenave, A., Mognard, N., Llovel, W., Frappart, F., 2011. Satellite-based high latitude snow volume trend, variability and contribution to sea level over 1989/2006. Glob. Planet. Change 75, 99–107. doi:10.1016/j.gloplacha.2010.10.011.

Brasnett, B., 1999. A global analysis of snow depth for numerical weather prediction. J. Appl. Meteorol. 38, 726–740.

Brown, R., 2000. Northern Hemisphere snow cover variability and change, 1915–97. J. Clim. 13, 2339–2355.

Brown, R., Goodison, B., 1996. Interannual variability in reconstructed Canadian snow cover, 1915–1992. J. Clim. 9, 1299–1318.

Brown, R., Derksen, C., Wang, L., 2010. A multi-data set analysis of variability and change in Arctic spring snow cover extent, 1967–2008. J. Geophys. Res. 115, D16111. doi:10.1029/2010JD013975.

Bulygina, O., Razuvaev, V., Korshunova, N., 2009. Change in snow cover over northern Eurasia in the last decades. Environ. Res. Lett. 4, 045026. doi:10.1088/17489326/14/4/045026.

Campbell, G., 1977. An Introduction to Environmental Biophysics. Springer-Verlag, New York, 159 pp.

Castellví, F., Perez, P., Villar, J., Resell, J., 1996. Analysis of methods for estimating vapor pressure deficits and relative humidity. Agri. For. Meteorol. 82, 29–45.

Dery, S., Sheffield, J., Wood, E., 2005. Connectivity between Eurasian snow cover extent and Canadian snow water equivalent and river discharge. J. Geophys. Res. 110, D23106. doi:10.1020/2005JD006173.

Déry, S., Brown, R., 2007. Recent Northern Hemisphere snow cover extent trends and implication for the snow-albedo feedback. Geophys. Res. Lett. 34, L22504. doi:10.1029/2007GL031474.

Dye, D., 2002. Variability and trends in the annual snow-cover cycle in Northern Hemisphere land areas, 1972–2000. Hydrol. Proc. 16, 3065–3077. doi:10.1002/hyp.1089.

Dyer, J., Mote, T., 2002. Role of energy budget components on snow ablation from a mid-latitude prairie snowpack. Polar Geogr. 26, 87–115.

Dyer, J., Mote, T., 2006. Spatial variability and trends in observed snow depth over North America. Geophys. Res. Lett. 33, L16503. doi:10.1029/2006GL027258.

Dyer, J., Mote, T., 2007. Trends in snow ablation over North America. Int. J. Clim. 27, 739–748. doi:10.1002/joc.1426.

Foster, J., Robinson, D., Hall, D., Estilow, T., 2008. Spring snow melt timing and changes over Arctic lands. Polar Geogr. 31, 145–157.

Ge, Y., Gong, G., 2008. Observed inconsistencies between snow extent and snow depth variability at regional/continental scales. J. Clim. 21, 1066–1082. doi:10.1175/2007JCLI1829.1.

Global Soil Data Task, 2000. Global Soil Data Products CD-ROM (IGBP-DIS), CD-ROM, International Geosphere-Biosphere Programme, Data and Information System, Potsdam, Germany. Available from. Oak Ridge National Laboratory Distributed Active Archive Center, Oak Ridge, Tennessee, U.S.A.

Gong, G., Entekhabi, D., Cohen, J., Robinson, D., 2004. Sensitivity of atmospheric response to modeled snow anomaly characteristics. J. Geophys. Res. 109, D06107. doi:10.1029/2003JD004160.

Grippa, M., Kergoat, L., Le Toan, T., Mognard, N., Delbart, N., L'Hermitte, J., Vicente-Serrano, S., 2005. The impact of snow depth and snowmelt on the vegetation variability over central Siberia. Geophys. Res. Lett. 32, L21412. doi:10.1029/2005GL024286.

Groisman, P., Karl, T., Knight, R., 1994. Changes of snow cover, temperature, and radiative heat balance over the Northern Hemisphere. J. Clim. 7, 1633–1656.

Groisman, P., Knight, R., Razuvaev, V., Bulygina, O., Karl, T., 2006. State of the ground: climatology and changes during the past 69 years over Northern Eurasia for a rarely used measure of snow cover and frozen land. J. Clim. 19, 4933–4955.

Hirabayashi, Y., Kanae, S., Struthers, I., Oki, T., 2005. A 100-year (1901–2000) global retrospective estimation of terrestrial water cycle. J. Geophys. Res. 110. doi:10.1029/2004JD005492.

Hirabayashi, Y., Kanae, S., Motoya, K., Masuda, K., Doll, P., 2008. A 59-year (1948–2006) global near-surface meteorological data set for land surface models. Part I: Development of daily forcing and assessment of precipitation intensity. Hydrol. Res. Lett. 2, 36–40.

Howell, S., Duguay, C., Markus, T., 2009. Sea ice conditions and melt season duration variability within the Canadian Arctic Archipelago: 1979–2008. Geophys. Res. Lett. 36, L10502. doi:10.1029/2009GL037681.

Iijima, Y., Fedorov, A., Park, H., Suzuki, K., Yabuki, H., Maximov, T., Ohata, T., 2010. Abrupt increases in soil temperatures following increased precipitation in a permafrost region, central Lena river basin, Russia. Permafrost Periglac. Process 21, 30–41.

Isard, S., Angel, J., VanDyke, G., 2000. Zones of origin for great Lakes cyclones in north America, 1899–1996. Mon. Wea. Rev. 128, 474–485.

Jordan, R., 1991. A one-dimensional temperature model for a snow cover: Technical documentation for SNTHERM.89. U.S. Army Cold Regions Research and Engineering Laboratory. Spec. Rep., 91–116.

Kitaev, L., Forland, E., Razuvaev, V., Tveito, O., Krueger, O., 2005. Distribution of snow cover over Northern Eurasia. Nord. Hydrol 36, 311–319.

Lindsay, R., Zhang, J., Schweiger, A., Steele, M., Stern, H., 2009. Arctic sea ice retreat in 2007 follows thinning trend. J. Clim. 22, 165–176.

Llody, a., Fastie, C., 2002. Spatial and temporal variability in the growth and climate response of treeline trees in Alaska. Clim. Change 52, 481–509.

McDonald, K., Kimball, J., Njoku, E., Zimmermann, R., Zhao, M., 2004. Variability in springtime thaw in the terrestrial high latitudes: monitoring a major control on the biospheric assimilation of atmospheric CO_2 with spaceborne microwave remote sensing. Earth Interact 8, 1–20.

Meador, W., Weaver, W., 1980. Two-stream approximations to radiative transfer in planetary atmospheres: a unified description of existing methods and a new improvement. J. Atmos. Sci. 37, 630–643.

Nelson, F., Shiklomanov, N., Mueller, G., Hinkel, K., Walker, D., Bockheim, J., 1997. Estimating active-layer thickness over a large region: Kuparuk River basin, Alaska, U.S.A. Arct. Alp. Res. 29 (4), 367–378.

Park, H., Iijima, Y., Yabuki, H., Ohta, T., Walsh, J., Kodama, Y., Ohata, T., 2011. The application of a coupled hydrological and biogeochemical model (CHANGE) for modeling of energy, water, and CO_2 exchanges over a larch forest in eastern Siberia. J. Geophys. Res. 116, D15102. doi:10.1029/2010JD015386.

Pomeroy, J., Marsh, P., Gray, D., 1997. Application of a distributed blowing snow model to the Arctic. Hydrol. Process. 11, 1451–1464.

Pomeroy, J., Li, L., 2000. Prairie and Arctic areal snow cover mass balance using a blowing snow model. J. Geophys. Res. 105 (D21), 26,619–26,634.

Ramankutty, N., Foley, J., 1999. Estimating historical changes in global land cover: Croplands from 1700 to 1992. Glob. Biogeochem. Cycles 13 (4), 997–1027.

Robinson, D., Dewey, K., Heim, R., 1993. Global snow cover monitoring: an update. Bull. Am. Meteorol. Soc. 74, 1689–1696.

Saito, K., Cohen, J., 2003. The potential role of snow cover in forcing interannual variability of the major Northern Hemisphere mode. Geophys. Res. Lett. 30, 1302. doi:10.1029/2002GL016341.

Saito, K., Yasunari, T., Cohen, J., 2004. Changes in the sub-decadal co-variability between Northern Hemisphere snow cover and the general circulation of the atmosphere. Int. J. Clim. 24, 33–44.

Screen, J., Simmonds, I., 2010. The central role of diminishing sea ice in recent Arctic temperature amplification. Nature 464 (29). doi:10.1038/nature09051.

Serreze, M., Bromwich, D., Clark, M., Etringer, A., Zhang, T., Lammers, R., 2003. Large-scale hydro-climatology of the terrestrial Arctic drainage system. J. Geophys. Res. 108 (D2), 8160. doi:10.1029/2001JD000919.

Serreze, M., Francis, J., 2006. The polar amplification debate. Clim. Change 76, 241–264.

Stieglitz, M., Dery, S., Romanovsky, V., Osterkamp, T., 2003. The role of snow cover in the warming of Arctic permafrost. Geophys. Res. Lett. 30 (13), 1721. doi:10.1029/2003GL017337.

Storck, P., Lettenmaier, D., Bolton, S., 2002. Measurement of snow interception and canopy effects on snow accumulation and melt in a mountainous maritime climate, Oregon, United States. Water Resour. Res. 38. doi:10.1029/2002WR001281 2002.

Wigmosta, M., Lettenmaier, D., 1994. A distributed hydrology-vegetation model for complex terrain. Water Resour. Res. 30, 1665–1679.

Yang, D., Robinson, D., Zhao, Y., Estilow, T., Ye, B., 2003. Streamflow response to seasonal snow cover extent changes in large Siberian watersheds. J. Geophys. Res. 108 (D18), 4578. doi:10.1029/2002JD003149.

Ye, H., 2001. Increases in snow season length due to earlier first snow and later last snow dates over North Central and Northwest Asia during 1937–94. Geophys. Res. Lett. 28 (3), 551–554.

NiPR
National Institute of Polar Research

INTERNATIONAL POLAR YEAR
2007-2008